Demystifying freeze-in dark matter at the LHC

Kyu Jung Bae,[1,2,*] Myeonghun Park,[1,3,†] and Mengchao Zhang[4,1,‡]

[1]*Center for Theoretical Physics of the Universe, Institute for Basic Science, Daejeon 34126, Korea*
[2]*Department of Physics, Kyungpook National University, Daegu 41566, Korea*
[3]*Institute of Convergence Fundamental Studies and School of Liberal Arts,*
Seoultech, 232 Gongneungro, Nowon-gu, Seoul 01811, Korea
[4]*Department of Physics and Siyuan Laboratory, Jinan University,*
Guangzhou 510632, People's Republic of China

Freeze-in mechanism provides robust dark matter production in the early Universe. Because of its feeble interactions, freeze-in dark matter leaves signals at colliders which are often involved with long-lived particle decays and consequent displaced vertices (DV). In this paper, we develop a method to read off mass spectrum of particles being involved in the DV events at the LHC. We demonstrate that our method neatly works under limited statistics, detector resolution, and smearing effects. The signature of DV at the LHC can come from either highly suppressed phase space or a feeble coupling of particle decay processes. By measuring invisible particle mass spectrum, one can discriminate these two cases and thus extract information of dominant freeze-in processes in the early Universe at the LHC.

I. INTRODUCTION

Particle dark matter (DM) is strongly supported by a plethora of cosmological and astrophysical evidences (for reviews on particle dark matter see Refs. [1–3]). Since there is no proper candidate of DM in the standard model (SM), it is considered as one of the most prominent clues to go beyond the SM. The freeze-in mechanism provides a plausible answer to the origin of particle DM in the primeval Universe [4], and also an intriguing set of DM searches in a broad area (e.g., nonthermal distribution of DM and its impacts [5–10], DM direct detection [11,12], and the large hadron collider (LHC) searches [13–16])[1] although it generically contains tiny interactions with visible particles.

On the contrary to the conventional freeze-out dark matter, freeze-in dark matter never reaches equilibration with thermal plasma. Because of its tiny interaction strength, instead, DM annihilation processes are always inefficient and thus the produced DM particles are accumulated as the Universe expands. Hence the correct DM abundance can be achieved despite of the feeble interactions [4]. Moreover, the production processes involve dimensionless couplings, so they become more important at low temperature and consequently a dominant number of DM particles are produced near the threshold mass scale of the production processes. Below the threshold scale, the production processes are highly suppressed by the Boltzmann factor. Therefore, the DM abundance is independent of high temperature physics, i.e., reheating after the primordial inflation, but is dependent on details of the production processes which are determined by the DM particle interactions.

The feeble nature of DM implies another observable footprint if the DM mass is $\mathcal{O}(1)$ keV. Since the DM particles are not equilibrated after being produced, their initial phase space distribution does not change but is simply redshifted during the cosmic expansion. As pointed out in the literature [9,10], phase space distribution of DM depends on mass spectrum, relative interaction strengths, and also its production channels such as two-body decay, three-body decay, s-channel, and t-channel scattering. In many cases, these production channels originate from the same interaction, so the mass spectrum of particles involved in the production processes determines which process is the dominant one as well as how warm the phase space distribution is. Such nonthermal distribution of DM particles impacts on small scale structures and can be probed by the Ly-α forest observation [18–25].

Along with the cosmology, collider study can provide a possible probe of the freeze-in dark matter model. During

---

[*]kyujung.bae@knu.ac.kr
[†]parc.seoultech@seoultech.ac.kr
[‡]mczhang@jnu.edu.cn
[1]For more broad aspects of freeze-in dark matter, readers can find reviews in Ref. [17].

the freeze-in processes, DM particles come out from thermal plasma of nonfeeble particles via feeble interactions between the dark sector and visible sector. It implies the events at colliders where nonfeeble particles are produced in pairs and decay into freeze-in DM particles plus visible particles. These events are indeed a direct reflection of the freeze-in dark matter production from decay of particles in thermal equilibrium. For example, Higgsino pairs are produced and decay into axinos and Higgs bosons. In virtue of its tiny coupling, such decays may show a signature of the displaced vertex (DV) at hadron colliders.[2] The DV searches at the LHC have been considered to investigate various long-lived particles and have increased the sensitivity. In addition, a possible improvement at the high-luminosity (HL) LHC with precision timing information would suppress SM backgrounds leading to a better sensitivity of such long-lived particle searches [27,28].

In order to examine genuine properties of the freeze-in dark matter model at hadron colliders, we need to go one step further. The DM abundance and distribution are determined by the couplings and mass spectrum of the dark sector including the DM component. Thus it is essential to extract the mass information from DV events at colliders. In the case of prompt decay events, kinematic analyses require a large number of events to read off the endpoint in the invariant mass distribution [29]. As pointed out in the early study [30,31], on the other hand, DV renders the mass reconstruction possible in an event-by-event basis, so it allows us to extract the mass spectrum of the dark sector although a handful of events are available. In reality, however, a kinematic reconstruction in an event-by-event basis highly depends on detector effects including smearing of final state visible particles.

In this paper, we present a collider method to reconstruct the mass spectrum related to the freeze-in processes with only conventional track and calorimeter information. To reduce uncertainties in mass measurement originating from detector smearing effects, we develop a simple "filtering" algorithm, which systematically discards the outliers in mass measurement of DV events. For an illustration of our method, we consider a pair production of mother particles (F) and their subsequent decays into dark matter particles (χ) and Z bosons, where Z boson decays into a lepton pair for a precise reconstruction.

This paper is organized as follows. In Sec. II, a brief review on freeze-in dark matter is given to argue why the long-lived particle at the LHC is appropriate to examine cosmological freeze-in dark matter scenarios. In Sec. III, we explain kinematic relations in events with DV to reconstruct masses of the decaying particle F and dark matter particle χ. In Sec. IV, we demonstrate how much a

simple filtering algorithm enhances accuracy by removing events that have strong smearing effects from a detector. Finally, we present our result in mass reconstructions with various benchmark points at the HL-LHC.

II. A BRIEF REVIEW ON FREEZE-IN DARK MATTER

In freeze-in dark matter models, DM particles have tiny *renormalizable* couplings with thermal plasma by which the freeze-in processes are mediated. In the following, we will explain the freeze-in mechanism with a toy example.

Suppose that DM particles are produced by decay of particle A, which is in thermal equilibrium, i.e., $A \rightarrow B + \chi$. Here we assume B is also in thermal equilibrium. In this case, a dark matter production rate is determined by the decay width of A, Γ_A. The dominant production occurs when the plasma temperature T is around m_A. For $T < m_A$, the population of A is highly suppressed by the Boltzmann factor, so the production process becomes ineffective. One finds the yield of DM particles [4,32],

$$
\begin{aligned}
Y_\chi &\approx \frac{135g}{4\pi^4 g_*^{3/2}} \frac{M_P \Gamma_A}{m_A^2} \int_0^\infty z^3 K_1(z) dz \\
&\approx 10^{-3} \frac{M_P \Gamma_A}{m_A^2},
\end{aligned}
\tag{2.1}
$$

where g is the degrees of freedom of A, g_* is the effective degrees of freedom of thermal plasma, M_P is the reduced Planck mass, and $K_1(z)$ is the first modified Bessel function of the second kind. In the second line, we have taken $g_* = 100$. For the decay of A via a renomarlizable coupling λ, the decay width is given by

$$
\Gamma_A \sim \frac{1}{8\pi} \lambda^2 m_A.
\tag{2.2}
$$

The yield becomes

$$
Y_\chi \sim 4 \times 10^{-5} \lambda^2 \frac{M_P}{m_A},
\tag{2.3}
$$

and the DM density is given by

$$
\begin{aligned}
\Omega_\chi h^2 &\sim 2.8 \times 10^8 Y_\chi \left(\frac{m_\chi}{\text{GeV}}\right) \\
&\sim 0.1 \left(\frac{\lambda}{10^{-8}}\right)^2 \left(\frac{200 \text{ GeV}}{m_A}\right) \left(\frac{m_\chi}{10 \text{ keV}}\right).
\end{aligned}
\tag{2.4}
$$

Therefore, one can see that the freeze-in process provides the correct DM abundance in a wide rage of couplings and DM masses although the coupling is tiny. For a coupling $\lambda \sim 10^{-8}$, a DM mass is of order keV, so it can be warm dark matter (WDM) and may be probed by small scale observables [5–10]. For an even smaller coupling,

---

[2]We refer readers to Ref. [26] for a recent review on long-lived particle searches at the LHC.

$\lambda \sim 10^{-12}$, on the other hand, a weak scale DM mass (~ 100 GeV) is possible so that the DM can be cold dark matter (CDM).

In most of freeze-in DM models, scattering processes are also accompanied by the decay processes. One can find a process like $A + C \rightarrow \chi + D$ (t-channel mediated by B) where C and D are also in thermal equilibrium. The single processes are normally less effective than the decay processes due to the suppression in the kinematic phase factor. In some cases, nonetheless, the scattering process can be enhanced by large numbers of degrees of freedom of accompanying particles C and D, so it can make sizable contributions to the DM production (see Refs. [33,34] for axino production cases). In addition, there may exist decay processes with more than 2 final state particles. However, this contribution is more suppressed than two-body decays by the kinematic phase factor, so is typically subdominant.

In the case where decay and scattering processes are "co-resident," more interestingly, a mass difference between A and B can determine a relative ratio between the decay and scattering contributions as well as the phase space distribution. In principle, if $m_A - m_B \ll m_A$, a kinetic energy of the produced DM can be arbitrarily small. Under these circumstances, a decay process become very inefficient. Nevertheless, a scattering process does not alter dramatically, so it dominates the phase space distribution and relic abundance [10]. Extracting a mass spectrum at collider experiments may enable us to infer which process is dominant in the freeze-in DM production.

At colliders, the direct production of χ is impossible since its couplings to SM particles are too small. However, its mother particle (A, in the above example) can be produced in the collision experiments. If A is the lightest parity-odd particle in the visible sector (e.g., Higgsino in the minimal supersymmetric standard model), it can decay only to a DM particle with a decay width in Eq. (2.2). The decay length at the collider is

$$\frac{1}{\Gamma_A} \sim (1.7 \text{ ns} \quad \text{or} \quad 50 \text{ cm}) \times \left(\frac{10^{-8}}{\lambda}\right)^2 \left(\frac{200 \text{ GeV}}{m_A}\right). \quad (2.5)$$

For the freeze-in DM with $m_\chi \sim 10$ keV and $\lambda \sim 10^{-8}$, a DV length is of order 10 cm, and thus this gives nearly the best sensitivity for DV searches at the LHC [35] while it gives the dominant dark matter abundance.

For a larger dark matter mass, $m \sim 100$ GeV, a smaller coupling $\lambda \sim 10^{-12}$ is required to obtain the correct relic abundance in the standard cosmology. If this is the case, the decay length is too long to be covered by DV searches. Such a region, instead, may be covered by an additional long-lived particle detector outside of the LHC detectors [36]. However, even in the case of large dark matter mass, there are viable nonstandard cosmological scenarios leading to the correct relic abundance. If a dark matter mass is around 100 GeV and a coupling is of order 10^{-8}, the

freeze-in process overproduces DM particles. In such a case, a large entropy dilution of a factor 10^7–10^8 is necessary to suppress the freeze-in processes properly. In a scenario where the DM freeze-in occurs during an early matter dominated era (i.e., $T_R \ll 100$ GeV), a relatively large coupling $\lambda \sim 10^{-8}$ still provides a viable DM scenario with the correct relic DM abundance [37]. In a scenario in the fast-expanding Universe [38], a similar dilution effect is possible so that a viable freeze-in DM model is possible with $m_\chi \sim 100$ GeV and $\lambda \sim 10^{-8}$. In another freeze-in DM model [5,6], DM particles can be produced by decays of frozen-out particles rather than directly produced from the thermal plasma. In such a case, DV searches at the LHC cover the freeze-in DM in an indirect way by showing the kinematic structure of particles decaying into the DM particle.

In summary, the current and future DV searches for decay length of order 10 cm will be good probes of the freeze-in WDM region and part of heavy freeze-in DM models. Once we observe an excess of DV signals above the expected background in the future, analyses on mass spectrum by using the kinematic techniques will be essential to reflect the DM production process in the early Universe. In the next section, we show kinematic relations to reconstruct masses of the mother particle and dark matter particle.

III. KINEMATICS OF DISPLACED VERTEX

We consider a case where the LHC produces pairs of unstable particles F. Each particle decays into dark matter χ and Z boson. To demonstrate this process, we consider an effective Lagrangian,

$$\mathcal{L} \ni \frac{1}{\Lambda^2} \bar{F} F \bar{q} q + (\epsilon Z_\mu \bar{F} \gamma^\mu P_L \chi + \text{H.c.}), \quad (3.1)$$

where F and χ are Majorana fermions, and q is a standard model quark. It must be noted that F is the lightest neutral component of two weak doublets while χ is a weak singlet. Such an interaction is realized by a singlet-doublet mixing that is encoded in the small coupling constant ϵ.[3] There are also a charged partner $F^\pm$ and a neutral partner F'. If $F^\pm$ and F' are slightly heavier than F by the mass difference $\Delta m = m_{F^\pm, F'} - m_F \simeq \mathcal{O}(10)$ GeV,[4] they promptly decay into the lightest neutral component F plus soft leptons or jets via a virtual $W^\pm$ or Z boson. While it is hard to detect

---

[3]In analogy, one can consider two Higgsino doublets and an axino.

[4]The $\mathcal{O}(10)$ GeV mass difference can be generated by a mixing with another singlet (other than the DM particle) whose mass is not much larger than the mass of F. In the case of supersymmetric models, bino can play a role of the singlet leading to a substantial mass splitting between Higgsino states. In the absence of such a mixing with a singlet, the electroweak correction generates an $\mathcal{O}(100)$ MeV mass splitting [39].
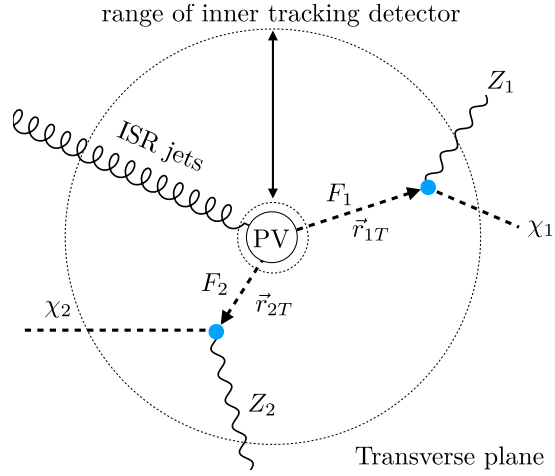
FIG. 1. Positions of two DVs are denoted by $\vec{r}_1$ and $\vec{r}_2$ (dashed arrows). Visible (reconstructable) particles are marked with solid lines while invisible particles with dashed ones. Dotted circles represents inner and outer boundary of "inner tracking detector (ID)" with cylindrical radius of $\mathcal{O}(10) - \mathcal{O}(10^3)$ mm; primary vertex (PV).

such heavy states due to the difficulty of tagging soft particles,[5] production of $F^{\pm}$ and F' can inclusively contribute to the pair production of the lightest neutral state F. The inclusive production channels such as $(F^{\pm}, F^{\mp})$ and $(F^{\pm}, F)$ can enhance the number of signal events under our consideration. These contributions are taken into account in the coupling $1/\Lambda^2$ when recasting current ATLAS results [35] in Sec. IV.

In our study, we focus on a method to identify the mass spectrum of (F, χ) in the event-by-event basis. This method is advantageous for extracting mass information compared to traditional methods with invariant mass or transverse mass variables which require large number of signal events as they utilize the *endpoint* of differential distributions.[6] In virtue of the information from displaced vertices, one can extract (m_F, m_χ) from a single event in an ideal situation. In reality, however, $\mathcal{O}(10)$ events are required to reduce various systematics including detector effects. In order to implement this method, we reconstruct four-momenta of dark matter particles (χ_i, $i = 1, 2$ for both sides). As the number of unknowns from χ_i is eight in total, we need to have the same number of constraints using kinematics.

At the LHC detector, F_i leave a DV, denoted by $\vec{r}_i$, when it decays into $Z_i (\to \ell^+\ell^-)$ and χ_i as in Fig. 1. Because of the charge neutrality of F_i, a three-momentum vector $\vec{p}_{F_i}$ is proportional to $\vec{r}_i$. This provides two constraints for the direction of each $\vec{p}_{(F_i)}$, resulting in four constraints in total.

_____

[5]For these heavy states, a few search strategies and bounds are summarized in a recent review [40].
[6]For more general reviews on traditional methods, we refer readers to Refs. [41,42].

If we specify a direction of DV in a spherical coordinate ($\hat{r}_i$: unit vector directing $\vec{r}_i$),

$$\hat{r}_i = (\sin\theta_i \cos\phi_i, \sin\theta_i \sin\phi_i, \cos\theta_i), \quad (3.2)$$

we can express three-momentum $\vec{p}_{(F_i)}$ in terms of DV position vector $\hat{r}_i$,

$$\vec{p}_{(F_i)} = |\vec{p}_{(F_i)}|\hat{r}_i. \quad (3.3)$$

In conventional searches for dark matter at the LHC, we utilize a momentum conservation in the transverse plane as we do not see the trace of dark matter directly. Thus, we have two constraints:

$$\vec{P}_T = \sum_i \vec{p}_{T(\chi_i)} = -\left(\vec{p}_{T(\mathrm{ISR})} + \sum_i \vec{p}_{T(Z_i)}\right). \quad (3.4)$$

This can be simply translated into a condition for $\vec{p}_{(F_i)}$:

$$\sum_i \vec{p}_{T(F_i)} = -\vec{p}_{T(\mathrm{ISR})}. \quad (3.5)$$

The existence of ISR jets is important to identify dark matter at the LHC. For example, ISR jets are required for the most conventional dark matter searches [43,44] and for utilizing information from a timing layer [27,28]. For the case of $\mathcal{O}(100\text{–}1000)$ GeV mass scale of F, there are non-negligible numbers of events with $p_{T(\mathrm{ISR})} \simeq \mathcal{O}(10\text{–}100)$ GeV [45,46] and we can utilize this information to extract properties of dark matter at the LHC [47,48]. In our case, we use $p_{T(\mathrm{ISR})}$ to reconstruct three-momenta $\vec{p}_{T(F_i)}$ by combining Eqs. (3.3) and (3.5),

$$\sum_i (|\vec{p}_{T(F_i)}|\hat{r}_{iT}) = -\vec{p}_{T(\mathrm{ISR})}. \quad (3.6)$$

In a more specific way, the above equation can be expressed by a 2×2 matrix equation,

$$\begin{pmatrix} \sin\theta_1 \cos\phi_1 & \sin\theta_2 \cos\phi_2 \\ \sin\theta_1 \sin\phi_1 & \sin\theta_2 \sin\phi_2 \end{pmatrix} \begin{pmatrix} |\vec{p}_{T(F_1)}| \\ |\vec{p}_{T(F_2)}| \end{pmatrix}$$
$$= -\begin{pmatrix} |\vec{p}_{T(\mathrm{ISR})}| \cos\phi \\ |\vec{p}_{T(\mathrm{ISR})}| \sin\phi \end{pmatrix}, \quad (3.7)$$

where ϕ is the azimuthal angle of $\vec{p}_{T(\mathrm{ISR})}$ in the transverse plane. This provides a solution for $|\vec{p}_{T(F_i)}|$ in terms of directional angles (ϕ_i, θ_i) of DVs,

$$|\vec{p}_{(F_1)}| = -\frac{|\vec{p}_{T(\mathrm{ISR})}| \sin(\phi - \phi_2)}{\sin\theta_1 \sin(\phi_1 - \phi_2)},$$

$$|\vec{p}_{(F_2)}| = \frac{|\vec{p}_{T(\mathrm{ISR})}| \sin(\phi - \phi_1)}{\sin\theta_2 \sin(\phi_1 - \phi_2)}. \quad (3.8)$$
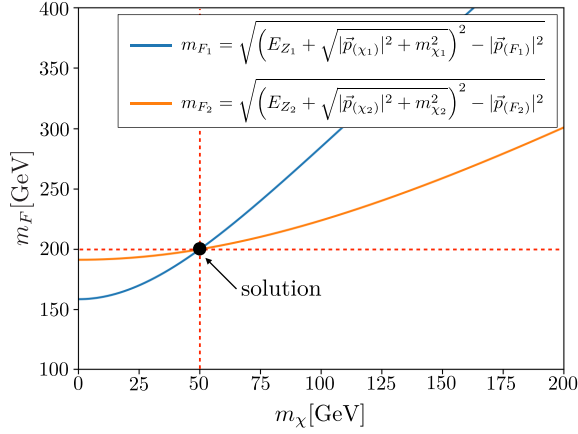
FIG. 2.   The functional dependence of m_{F_i} on m_{χ_i} in a specific event is presented as blue and magenta lines according to Eq. (3.11). The event is generated at the parton level with a study point of $(m_F, m_\chi) = (200, 50)$ GeV. For $m_{F_1} = m_{F_2}$ and $m_{\chi_1} = m_{\chi_2}$, the crossing point of two equations gives the solution for m_F and m_χ.

When the ISR jet becomes soft, Eq. (3.7) turns into an indeterminate system. In the limit of $p_{T(\mathrm{ISR})} \ll \sqrt{\hat{s}}$, where $\sqrt{\hat{s}}$ is the hard scale of an event, the difference $\phi_1 - \phi_2$ can be approximately expressed by

$$\phi_1 - \phi_2 \simeq \pi - \frac{2p_{T(\mathrm{ISR})}}{\sqrt{\hat{s}}} \left(1 - \frac{4m_F^2}{\hat{s}}\right)^{-\frac{1}{2}} \to \pi. \qquad (3.9)$$

As Eq. (3.7) has a factor $\sin(\phi_1 - \phi_2)$ in its determinant, it is required to have non-negligible $p_{T(\mathrm{ISR})}$ to have a numerically stable solution for $|\vec{p}_{(F_i)}|$.

To extract information on masses of invisible particles, we convert the solution of momenta into the masses using the energy conservation as

$$\sqrt{m_{F_i}^2 + |\vec{p}_{(F_i)}|^2} = E_{Z_i} + \sqrt{m_{\chi_i}^2 + |\vec{p}_{(\chi_i)}|^2}. \qquad (3.10)$$

From this, we have a functional dependence of m_{F_i} on m_{χ_i} as

$$m_{F_i} = \sqrt{\left(E_{Z_i} + \sqrt{|\vec{p}_{(\chi_i)}|^2 + m_{\chi_i}^2}\right)^2 - |\vec{p}_{(F_i)}|^2}. \qquad (3.11)$$

Here the three-momentum of χ_i is given by $\vec{p}_{(\chi_i)} = |\vec{p}_{(F_i)}|\hat{r}_i - \vec{p}_{(Z_i)}$. So far we have used only six constraints to reconstruct three-momenta of $\vec{p}_{(F_i)}$. We can have two more constraints from our physics motivation where we assume the symmetric condition of $m_{F_1} = m_{F_2}$ and $m_{\chi_1} = m_{\chi_2}$. Thus we have eight constraints which suffice to measure (m_F, m_χ) even with one event. To illustrate how one can use Eq. (3.11), we take an event with $(m_F, m_\chi) = (200, 50)$ GeV. In Fig. 2, each function for

m_{F_i} in Eq. (3.11) is presented either as a blue or orange line with a crossing point as the solution for (m_F, m_χ).

IV. THE HL-LHC STUDY

A. Detector effects with a limited number of events

We consider a channel where DVs can be marked by tracing leptonically decaying Z bosons, i.e., $Z \to \ell^+\ell^-$ This channel is superior to hadronically decaying Z due to the clean lepton tracks. At the LHC, however, uncertainties still remain in (i) the measurements of lepton momenta, which can be modeled with 2% uncertainty [49,50], (ii) the DV position resolution with a conservative value of 0.5 mm [51], and (iii) the missing transverse energy $\not{E}_T$ resolution of 10% in the region of $\not{E}_T > 200$ GeV [52]. These smearing effects will result in incorrect solutions to Eq. (3.11).

To numerically show the effects of the above uncertainties, we simulate events with the study point of $(m_F, m_\chi) = (200, 50)$ GeV using Monte Carlo simulations by modeling the smearing effects with Gaussian functions. As we discussed earlier, $p_{T(\mathrm{ISR})}$ can enhance the numerical stability against the smearing effects. We can observe this clearly in Fig. 3 where we divide Monte Carlo events according to the range of $p_{T(\mathrm{ISR})}$. In reality, however, we have only $\mathcal{O}(10)$ events after cuts at the HL-LHC and most of the events are located at low $p_{T(\mathrm{ISR})}$, so we are not able to rely on the high $p_{T(\mathrm{ISR})}$ configurations. For this reason, we need to develop another method to reduce the smearing effects.

For this goal, we develop a simple "filtering" algorithm. Basically we rely on the fact that events are independent of one another. Thus we focus on the clustering structure of the solutions near the true mass point in (m_F, m_χ) solution space;

(i) Each solution is treated as a vector $\vec{v}_i$ at the $m_F - m_\chi$ plane with $\vec{v}_i = (m_{Fi}, m_{\chi i})$.
(ii) For each $\vec{v}_i$, we measure an "average distance" d_i,

$$d_i = \frac{1}{N} \sum_{j=1}^{N} |\vec{v}_i - \vec{v}_j|, \qquad (4.1)$$

where N is the total number of solution vectors,
(iii) remove the $\vec{v}_i$ with largest d_i from our vector list,
(iv) calculate all d_i again (only use the remaining vectors), and remove the vector with largest average distance. Repeat this process until only half of the vectors remain.

This filtering algorithm is neatly dropping bad solutions in a simple and systematic way as in Fig. 4.

B. Numerical studies with benchmark points

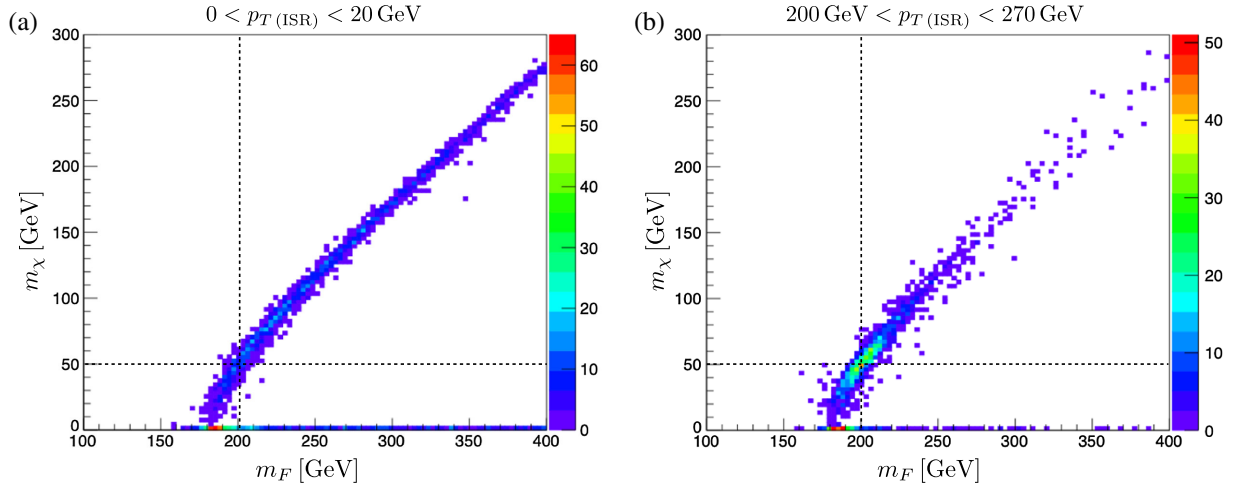In order to examine our method with realistic data at the HL-LHC, we consider four benchmark points for

FIG. 3. Distribution of solutions in Eq. (3.11) for a mass spectrum $(m_F, m_\chi) = (200, 50)$ GeV with (a) $0 < p_{T(\text{ISR})} < 20$ GeV and (b) 20 GeV $< p_{T(\text{ISR})} < 270$ GeV. We use 2000 events for each $p_{T(\text{ISR})}$ region using standard parton-level Monte Carlo simulations with Gaussian smearing for detector effects.
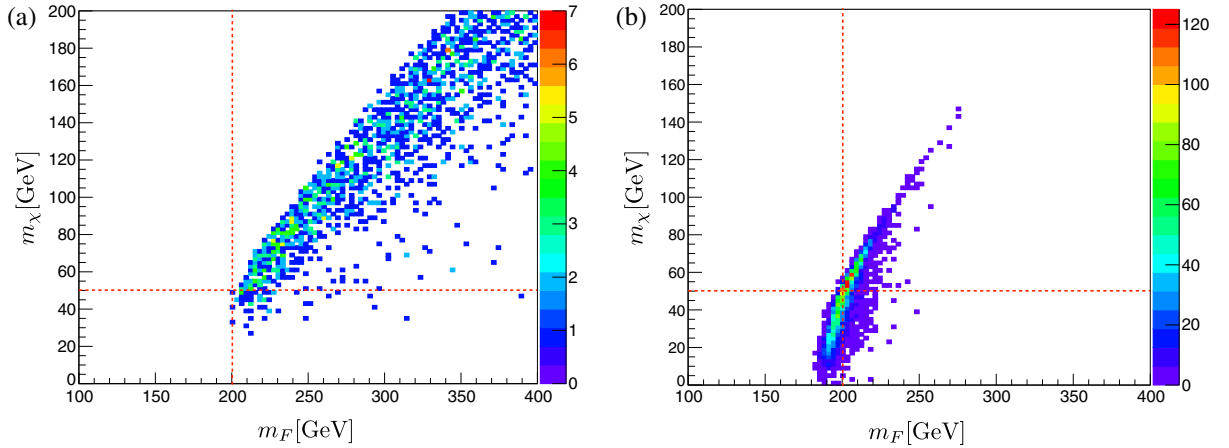

FIG. 4. We show the result of 5000 pseudoexperiments (a) without and (b) with the filtering algorithm. We have only 20 events per one pseudoexperiment. For each experiment, we take the mean values for mass measurement. The mass spectrum is the same as in Fig. 3.

different scales of m_F and mass gaps, which are listed in Table I. For benchmark points B and D, the mass gaps are highly suppressed, i.e., $\{m_F - (m_\chi + m_Z)\}/m_F \leq \mathcal{O}(1)\%$ while the mass gaps are more than 50% for A and C. Thus if we measure the mass spectrum (m_F, m_χ) precisely, we can learn the origin of long lifetime of F: either a suppressed phase space of small mass gap or a tiny coupling of $F - \chi - Z$. We consider the same lifetime of F ($c\tau = 100$ mm) for all benchmark points to focus on the kinematic differences and the performance of our method, which relies only on the reconstruction of $\vec{p}_{(F_i)}$, By recasting the current long-lived particle search of ATLAS [35], we expect 30, 20, 12, and 24 events, respectively, for benchmark point A, B, C, and D at the HL-LHC. We describe detailed information of the recasting procedure in Appendix A.

For the parton-level Monte Carlo simulations, we use MadGraph5 [53] to generate events with the "MLM" jet matching algorithm [54] implemented in PYTHIA8 [55] for ISR jets. To cluster ISR jets, we use FASTJET [56] with the

TABLE I. Four benchmark points (B.P.) are illustrated. As the LHC detector is not sensitive to probe a mass scale less than $\mathcal{O}(1)$ GeV, we fix $m_\chi = 0$ for the mass scale of $\mathcal{O}(1 - 100)$ keV. N_{events} is determined by recasting current LHC searches. These numbers are after baseline selection cuts.

B. P.	m_F [GeV]	m_χ [GeV]	$c\tau$ (mm)	N_{events} @ HL-LHC
A	200	0	100	30
B	200	108	100	20
C	800	0	100	12
D	800	708	100	24

anti-k_t algorithm [57]. For the detector effects, we consider detector geometries and smearing effects as we described above. Finally, we choose 14 TeV collision energy and 3 ab^{-1} luminosity for the HL-LHC. As we need to enhance precision for DV, we focus only on the leptonic decay of Z bosons. For the baseline selection cuts, we require

  (i) missing transverse energy $\not{E}_T > 200$ GeV to improve the $\not{E}_T$ resolution [52],

 (ii) 4 electrons or muons with $p_T > 10$ GeV in the final state,

(iii) 2 DVs to be reconstructed inside the inner detector (4 mm $< L_{xy} < 1$ m and $|L_z| < 1$ m) where DVs are reconstructed by displaced tracks with an impact parameter larger than 2 mm and $p_T > 1$ GeV, two tracks of each DV to be matched to 2 leptons, and both DV mass m_{DV} to be larger than 80 GeV.[7]

Since we require a moderate $\not{E}_T$, it is worth checking the corresponding cut efficiency. In our Monte Carlo simulations, we have $\epsilon_A \simeq 38\%$, $\epsilon_B \simeq 13\%$, $\epsilon_C \simeq 87\%$, and $\epsilon_D \simeq 15\%$, respectively, for benchmark cases A, B, C, and D. To understand this, we add $\not{E}_T$ distributions and corresponding explanations in the Appendix B.

Because of the detector effects and limited statistics, the mass measurement based on track information has large uncertainties. In order to improve the precision, we apply the filtering algorithm. It is worth mentioning a subtlety in solving Eq. (3.11) especially when dark matter is very light. There are cases where two lines in Fig. 2 do not cross due to the smearing effects. As $m_{F_i}(m_{\chi_i})$ is an increasing function, we take $m_\chi = 0$ and $m_F = (m_{F_1}(m_{\chi_1} = 0) + m_{F_2}(m_{\chi_2} = 0))/2$ for a solution.

For benchmark points in Table I, we perform 5000 pseudoexperiments to reduce statistical fluctuations. In Table II, we tabulate the most probable mass values for each benchmark point and also estimated statistical errors of pseudoexperiments which are defined by the root mean square (rms) value with respect to the most probable values rms $= \sqrt{\sum_{i=1}^{N}(m_i - m^{\text{peak}})^2/N}$, where m^{peak} is the most probable value and N is the number of pseudoexperiments. For benchmark points A, B, and D, the results show good precisions, where the errors are around 10% of the mother particle masses. For benchmark point C, on the other hand, the rms error is around 30%–45% of the mother particle mass. This mainly comes from small statistics as C has only 12 events after cuts which has factor 1/2–1/3 reduction compared to other benchmark points.

In the following, we discuss a more direct implication of the above analyses in the freeze-in dark matter scenarios. As argued in Ref. [10], if the phase space of a mother particle decay is highly suppressed, the distribution of DM produced from this decay process becomes colder.

---

[7]It is not likely that background processes have $m_{DV} > 80$ GeV [35], so this cut leads background-free analyses.

TABLE II. Peak measured values and root mean squares for four benchmark points. Numbers are in units of GeV.

B. P.	$\dfrac{(m_F, m_\chi)^{\text{true}}}{(m_F, m_\chi)^{\text{peak}}}$	rms
A	(200, 0) (208, 14)	(7.3,13)
B	(200, 108) (199,105)	(14,15)
C	(800, 0) (835, 0)	(250,360)
D	(800, 708) (792, 694)	(79,80)

Meanwhile, the distribution of DM produced by two-to-two scattering processes remains almost the same. This feature can be probed by observations such as Ly-α forest data if the DM mass is of order keV. Therefore, by observing the mass spectrum of the DM sector at the LHC, we can infer the relative "warmness" of the DM distribution. In order to illustrate such a situation, we introduce an additional benchmark point E, on which $(m_F, m_\chi) = (100, 0)$ GeV, $c\tau = 100$ mm. The expected number of events after the baseline selection cuts at the HL-LHC is 10. At the LHC, we measure $(m_F, m_\chi)^{\text{peak}} = (101, 0)$ GeV with statistical deviation rms $= (81, 47)$ GeV from 5K pseudoexperiments. Thus, even though we have uncertainties in determining the mass spectrum due to the limited statistics, we will have hints of the dark matter temperature of our Universe from the HL-LHC.

V. CONCLUSIONS

We consider a pure kinematic method to determine the mass spectrum involving DVs at the LHC by locating visible particle tracks inside the inner tracking detector. To measure the mass spectrum, we assume conditions $(m_{F_1} = m_{F_2})$ and $(m_{\chi_1} = m_{\chi_2})$ for both decay chains. We also require ISR jets not to have a back-to-back configuration between F's which results in a null solution in reconstructing three-momentum vectors of F's. Large ISR can enhance the numerical stability when determining the mass spectrum, but we would not have enough statistics to focus on the large $p_{T(\text{ISR})}$ region at the HL-LHC.

In this study, our analyses contain only $\mathcal{O}(10)$ events with the detector smearing effects. The performance of the mass measurements gets degraded due to imprecise information on $\not{E}_T$ and four-momenta of the leptons. To achieve satisfactory performance with small number of events, we propose a simple and systematic method which removes solutions with large errors in the mass reconstruction.

We have demonstrated that one can achieve mass measurements within $\mathcal{O}(10)\%$-level precision at the HL-LHC. This result enables us to understand the origin of DV signals, either due to the suppressed phase space or

due to the feeble coupling of the decaying particle. In this respect, we can see a relationship between the freeze-in mechanism in the early universe and the DV signature at the LHC.

Finally, as we do not rely on any new features of upcoming detector upgrades, our proposed method is orthogonal to other studies utilizing timing information [27,28]. One can enhance the precision in mass measurements by combining results from both methods once the LHC identifies DV signals from new physics.

ACKNOWLEDGMENTS

APPENDIX A: RECASTING OF CURRENT LONG-LIVED PARTICLE SEARCHES

We recast the ATLAS long-lived massive particles search report [35] to estimate the upper limit of $\sigma(pp \to FF)$.[8] There are other long-lived particle searches, for example, searches with displaced jets in the ATLAS [61], which are insensitive to our scenario as they need information of calorimeters.

Here we briefly describe the cut flow used in the ATLAS report [35].

(i) Transverse missing energy $\not{E}_T \geq 250$ GeV.
(ii) 75% of events need to have at least one trackless jet with $p_T > 70$ GeV or at least two trackless jets with $p_T > 25$ GeV. For the other 25% of events there is no requirement on the trackless jet. Trackless jet is defined to be a jet with $\sum p_T^{\text{track}} < 5$ GeV.
(iii) At least one DV needs to be reconstructed in the fiducial region of the inner detector within a transverse position 4 mm $< L_{\text{xy}} < 300$ mm and longitudinal position $|L_z| < 300$ mm. DV is reconstructed by displaced tracks with impact parameters larger than 2 mm and $p_T > 1$ GeV. More than five displaced tracks (N_{tracks}) from a DV are required, and reconstructed mass with tracks from DV (m_{DV}) needs to be larger than 10 GeV.

---

[8]For our benchmark model, ATLAS DV search report [35] provides the best sensitivity. CMS neutral long-lived particle search reports [58–60] are sensitive to different signal categories of displaced jets and decay length around 1 m, which provide weaker constraints compared to the ATLAS study.

TABLE III. Acceptance, upper limits on production cross section at 13 TeV, and recasted cross section at 14 TeV LHC. Values are in units of fb.

B. P.	Acceptance	$\sigma(pp \to FF)^{\max}_{13\,\text{TeV}}$	$\sigma(pp \to FF)^{\max}_{14\,\text{TeV}}$
A	0.63%	14.43	17.56
B	0.14%	64.41	78.41
C	6.76%	1.35	1.87
D	0.52%	17.62	24.34

TABLE IV. Benchmark points by features of kinematics.

Category	$\Delta m/m_F < 1\%$	$\Delta m/m_F > 50\%$
Small m_F	B	A
Large m_F	D	C

(iv) 42% fiducial volume needs to be discarded due to huge backgrounds from hadronic interactions in a material rich region.

In order to simulate the ATLAS detector's response to long-lived particles, we utilize parametrized DV tagging efficiency grids in the auxiliary material[9] of Ref. [35] as suggested in the contribution 22 of Ref. [62]. With this grid, we obtain tagging efficiencies based on the generator level (truth level) information about position, track multiplicity N_{tracks}, and invariant mass m_{DV} of DV. This method has been proven to be reliable in Ref. [62]. Acceptances of our 4 benchmark points after performing above selection criteria are listed in Table III. Acceptances for compressed spectra B and D are much smaller than spectra with large mass gaps A and C since compressed spectra do not provide large enough $\not{E}_T$ which is shown in Fig 5.

APPENDIX B: THE BEHAVIOR OF $\not{E}_T$

Let us explain the behavior of $\not{E}_T$ distributions in Fig. 5 based on the kinematics. We consider four benchmark cases based on (i) mass gap $\Delta m \equiv m_F - (m_Z + m_\chi)$ and (ii) scale of m_F as summarized in Table IV. A mass gap Δm affects the magnitude of momentum $\vec{p}_{\chi_i}$ at the rest frame of F_i while a scale m_F controls the ISR distributions [48]. For compressed spectra of B and D, the $|\vec{p}_{\chi_i}|$ at the rest frame of F_i is $\mathcal{O}(10)$ GeV. Thus events with large ISR can have corresponding large $\not{E}_T$ by a boost on the (F_1, F_2) system from ISR. As the hard scale in D is larger than the hard scale in B, we have a slightly larger $\not{E}_T$ distribution in D than the one in B. In the cases of A and C where Δm is

---

[9]We refer readers to Tables 25–36 of HEP Data, (https://doi.org/10.17182/hepdata.78697.v2). This is also summarized in the document, Auxiliary information for paper SUSY-2016-08.
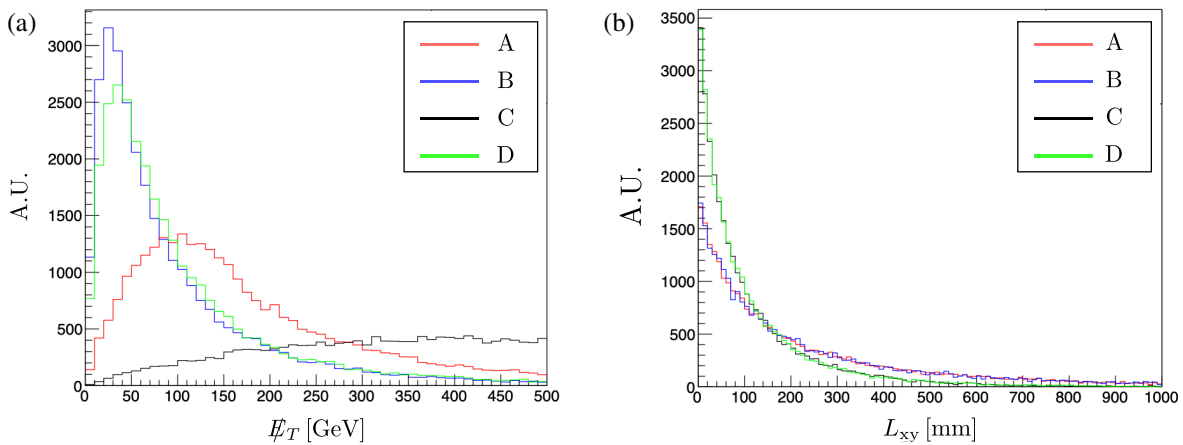
(a)

(b)

FIG. 5. Distributions of (a) $\not{E}_T$ and (b) L_{xy} for benchmark points. Benchmark points B and D with small mass splittings have lower $\not{E}_T$ distributions than those of A and C. For L_{xy}, C and D with larger m_F have smaller values than the case of A and B. N_{tracks} and m_{DV} distributions are not significantly different among benchmark points.

more than 50% of m_F, we have enough statistics with $\not{E}_T \gtrsim \mathcal{O}(100)$ GeV. At the rest frame of F_i, χ_i has $|\vec{p}_{\chi_i}| \sim 80$ GeV for A and $|\vec{p}_{\chi_i}| \sim 400$ GeV for C. $\not{E}_T$ is determined by the vector sum of $\vec{p}_{T(\chi_1)}$ and $\vec{p}_{T(\chi_2)}$ which are

independent. Thus the peak value of the $\not{E}_T$ distribution is around $|\vec{p}_{\chi_i}|$ at the rest frame of F_i. With a boost from ISR, the peak value of the $\not{E}_T$ distribution becomes slightly larger than $|\vec{p}_{\chi_i}|$ as shown in Fig. 5.

[1] G. Jungman, M. Kamionkowski, and K. Griest, Supersymmetric dark matter, Phys. Rep. **267**, 195 (1996).

[2] G. Bertone, D. Hooper, and J. Silk, Particle dark matter: Evidence, candidates and constraints, Phys. Rep. **405**, 279 (2005).

[3] G. Bertone and D. Hooper, History of dark matter, Rev. Mod. Phys. **90**, 045002 (2018).

[4] L. J. Hall, K. Jedamzik, J. March-Russell, and S. M. West, Freeze-in production of FIMP dark matter, J. High Energy Phys. 03 (2010) 080.

[5] A. Merle and M. Totzauer, keV sterile neutrino dark matter from singlet scalar decays: Basic concepts and subtle features, J. Cosmol. Astropart. Phys. 06 (2015) 011.

[6] J. König, A. Merle, and M. Totzauer, keV sterile neutrino dark matter from singlet scalar decays: The most general case, J. Cosmol. Astropart. Phys. 11 (2016) 038.

[7] S. B. Roland and B. Shakya, Cosmological imprints of frozen-in light sterile neutrinos, J. Cosmol. Astropart. Phys. 05 (2017) 027.

[8] J. Heeck and D. Teresi, Cold keV dark matter from decays and scatterings, Phys. Rev. D **96**, 035018 (2017).

[9] K. J. Bae, A. Kamada, S. P. Liew, and K. Yanagi, Colder freeze-in axinos decaying into photons, Phys. Rev. D **97**, 055019 (2018).

[10] K. J. Bae, A. Kamada, S. P. Liew, and K. Yanagi, Light axinos from freeze-in: production processes, phase space distributions, and Ly-α forest constraints, J. Cosmol. Astropart. Phys. 01 (2018) 054.

[11] R. Essig, J. Mardon, and T. Volansky, Direct detection of Sub-GeV dark matter, Phys. Rev. D **85**, 076007 (2012).

[12] T. Hambye, M. H. G. Tytgat, J. Vandecasteele, and L. Vanderheyden, Dark matter direct detection is testing freeze-in, Phys. Rev. D **98**, 075017 (2018).

[13] G. Barenboim, E. J. Chun, S. Jung, and W. I. Park, Implications of an axino LSP for naturalness, Phys. Rev. D **90**, 035020 (2014).

[14] A. G. Hessler, A. Ibarra, E. Molinaro, and S. Vogl, Probing the scotogenic FIMP at the LHC, J. High Energy Phys. 01 (2017) 100.

[15] L. Calibbi, L. Lopez-Honorez, S. Lowette, and A. Mariotti, Singlet-Doublet Dark Matter Freeze-in: LHC displaced signatures versus cosmology, J. High Energy Phys. 09 (2018) 037.

[16] G. Bélanger *et al.*, LHC-friendly minimal freeze-in models, J. High Energy Phys. 02 (2019) 186.

[17] N. Bernal, M. Heikinheimo, T. Tenkanen, K. Tuominen, and V. Vaskonen, The dawn of FIMP dark matter: A review of models and constraints, Int. J. Mod. Phys. A **32**, 1730023 (2017).

[18] M. Viel, J. Lesgourgues, M. G. Haehnelt, S. Matarrese, and A. Riotto, Constraining warm dark matter candidates including sterile neutrinos and light gravitinos with WMAP and the Lyman-alpha forest, Phys. Rev. D **71**, 063534 (2005).

[19] U. Seljak, A. Makarov, P. McDonald, and H. Trac, Can Sterile Neutrinos be the Dark Matter?, Phys. Rev. Lett. **97**, 191303 (2006).

[20] M. Viel, J. Lesgourgues, M. G. Haehnelt, S. Matarrese, and A. Riotto, Can Sterile Neutrinos be Ruled out as Warm Dark Matter Candidates?, Phys. Rev. Lett. **97,** 071301 (2006).

[21] M. Viel, G. D. Becker, J. S. Bolton, M. G. Haehnelt, M. Rauch, and W. L. W. Sargent, How Cold is Cold Dark Matter? Small Scales Constraints from the Flux Power Spectrum of the High-Redshift Lyman-Alpha Forest, Phys. Rev. Lett. **100,** 041304 (2008).

[22] M. Viel, G. D. Becker, J. S. Bolton, and M. G. Haehnelt, Warm dark matter as a solution to the small scale crisis: New constraints from high redshift Lyman-α forest data, Phys. Rev. D **88,** 043502 (2013).

[23] J. Baur, N. Palanque-Delabrouille, C. Yèche, C. Magneville, and M. Viel, Lyman-alpha forests cool warm dark matter, J. Cosmol. Astropart. Phys. 08 (**2016**) 012.

[24] V. Iršič et al., New Constraints on the free-streaming of warm dark matter from intermediate and small scale Lyman-α forest data, Phys. Rev. D **96,** 023522 (2017).

[25] C. Yèche, N. Palanque-Delabrouille, J. Baur, and H. du Mas des Bourboux, Constraints on neutrino masses from Lyman-alpha forest power spectrum with BOSS and XQ-100, J. Cosmol. Astropart. Phys. 06 (**2017**) 047.

[26] J. Alimena et al., Searching for long-lived particles beyond the Standard Model at the Large Hadron Collider, arXiv:1903.04497.

[27] J. Liu, Z. Liu, and L.-T. Wang, Enhancing Long-Lived Particles Searches at the LHC with Precision Timing Information, Phys. Rev. Lett. **122,** 131801 (2019).

[28] D. W. Kang and S. C. Park, Timing information at HL-LHC: Complete determination of masses of Dark Matter and Long lived particle, J. High Energy Phys. 03 (2020) 132.

[29] I. Hinchliffe, F. E. Paige, M. D. Shapiro, J. Soderqvist, and W. Yao, Precision SUSY measurements at CERN LHC, Phys. Rev. D **55,** 5520 (1997).

[30] M. Park and Y. Zhao, Recovering particle masses from missing energy signatures with displaced tracks, arXiv:1110.1403.

[31] G. Cottin, Reconstructing particle masses in events with displaced vertices, J. High Energy Phys. 03 (2018) 137.

[32] E. J. Chun, Dark matter in the Kim-Nilles mechanism, Phys. Rev. D **84,** 043509 (2011).

[33] K. J. Bae, K. Choi, and S. H. Im, Effective interactions of axion supermultiplet and thermal production of axino dark matter, J. High Energy Phys. 08 (2011) 065.

[34] K. J. Bae, E. J. Chun, and S. H. Im, Cosmology of the DFSZ axino, J. Cosmol. Astropart. Phys. 03 (2012) 013.

[35] M. Aaboud et al. (ATLAS Collaboration), Search for long-lived, massive particles in events with displaced vertices and missing transverse momentum in $\sqrt{s} = 13$ TeV pp collisions with the ATLAS detector, Phys. Rev. D **97,** 052012 (2018).

[36] D. Curtin et al., Long-lived particles at the energy frontier: The MATHUSLA physics case, Rep. Prog. Phys. **82,** 116201 (2019).

[37] R. T. Co, F. D'Eramo, L. J. Hall, and D. Pappadopulo, Freeze-in dark matter with displaced signatures at colliders, J. Cosmol. Astropart. Phys. 12 (2015) 024.

[38] F. D'Eramo, N. Fernandez, and S. Profumo, Dark matter freeze-in production in fast-expanding universes, J. Cosmol. Astropart. Phys. 02 (2018) 046.

[39] S. D. Thomas and J. D. Wells, Phenomenology of Massive Vectorlike Doublet Leptons, Phys. Rev. Lett. **81,** 34 (1998).

[40] H. Baer, V. Barger, S. Salam, D. Sengupta, and K. Sinha, Midi-review: Status of weak scale supersymmetry after LHC Run 2 and ton-scale noble liquid WIMP searches, arXiv:2002.03013.

[41] M. Burns, K. T. Matchev, and M. Park, Using kinematic boundary lines for particle mass measurements and disambiguation in SUSY-like events with missing energy, J. High Energy Phys. 05 (2009) 094.

[42] A. Barr, T. Khoo, P. Konar, K. Kong, C. Lester, K. Matchev, and M. Park, Guide to transverse projections and mass-constraining variables, Phys. Rev. D **84,** 095031 (2011).

[43] M. Aaboud et al. (ATLAS Collaboration), Search for new phenomena in final states with an energetic jet and large missing transverse momentum in pp collisions at $\sqrt{s} = 13$ TeV using the ATLAS detector, Phys. Rev. D **94,** 032005 (2016).

[44] CMS Collaboration, Search for new particles decaying to a jet and an emerging jet J. High Energy Phys. 02 (2019) 179.

[45] J. Alwall et al., Comparative study of various algorithms for the merging of parton showers and matrix elements in hadronic collisions, Eur. Phys. J. C **53,** 473 (2008).

[46] J. Alwall, K. Hiramatsu, M. M. Nojiri, and Y. Shimizu, Novel Reconstruction Technique for New Physics Processes with Initial State Radiation, Phys. Rev. Lett. **103,** 151802 (2009).

[47] J. L. Feng, S. Su, and F. Takayama, Lower Limit on Dark Matter Production at the Large Hadron Collider, Phys. Rev. Lett. **96,** 151802 (2006).

[48] K. J. Bae, T. H. Jung, and M. Park, Spectral Decomposition of Missing Transverse Energy at Hadron Colliders, Phys. Rev. Lett. **119,** 261801 (2017).

[49] G. Aad et al. (ATLAS Collaboration), Muon reconstruction performance of the ATLAS detector in proton–proton collision data at $\sqrt{s} = 13$ TeV, Eur. Phys. J. C **76,** 292 (2016).

[50] M. Aaboud et al. (ATLAS Collaboration), Electron and photon energy calibration with the ATLAS detector using 2015–2016 LHC proton-proton collision data, J. Instrum. **14,** P03017 (2019).

[51] ATLAS Collaboration, Performance of vertex reconstruction algorithms for detection of new long-lived particle decays within the ATLAS inner detector, Technical Report No. ATL-PHYS-PUB-2019-013, CERN, Geneva, 2019, https://cds.cern.ch/record/2669425.

[52] M. Aaboud et al. (ATLAS Collaboration), Performance of missing transverse momentum reconstruction with the ATLAS detector using proton-proton collisions at $\sqrt{s} = 13$ TeV, Eur. Phys. J. C **78,** 903 (2018).

[53] J. Alwall, R. Frederix, S. Frixione, V. Hirschi, F. Maltoni, O. Mattelaer, H. S. Shao, T. Stelzer, P. Torrielli, and M. Zaro, The automated computation of tree-level and next-to-leading order differential cross sections, and their matching to parton shower simulations, J. High Energy Phys. 07 (2014) 079.

[54] M. L. Mangano, M. Moretti, F. Piccinini, and M. Treccani, Matching matrix elements and shower evolution for top-quark production in hadronic collisions, J. High Energy Phys. 01 (2007) 013.

[55] T. Sjostrand, S. Mrenna, and P. Z. Skands, A brief introduction to PYTHIA 8.1, Comput. Phys. Commun. **178**, 852 (2008).

[56] M. Cacciari, G. P. Salam, and G. Soyez, FastJet user manual, Eur. Phys. J. C **72**, 1896 (2012).

[57] M. Cacciari, G. P. Salam, and G. Soyez, The anti-k_t jet clustering algorithm, J. High Energy Phys. 04 (2008) 063.

[58] A. M. Sirunyan *et al.* (CMS Collaboration), Search for long-lived particles decaying into displaced jets in proton-proton collisions at $\sqrt{s} = 13$ TeV, Phys. Rev. D **99**, 032011 (2019).

[59] A. M. Sirunyan *et al.* (CMS Collaboration), Search for long-lived particles using nonprompt jets and missing transverse momentum with proton-proton collisions at $\sqrt{s} = 13$ TeV, Phys. Lett. B **797**, 134876 (2019).

[60] A. M. Sirunyan *et al.* (CMS Collaboration), Search for new particles decaying to a jet and an emerging jet, J. High Energy Phys. 02 (2019) 179.

[61] M. Aaboud *et al.* (ATLAS Collaboration), Search for long-lived neutral particles in pp collisions at $\sqrt{s} = 13$ TeV that decay into displaced hadronic jets in the ATLAS calorimeter, Eur. Phys. J. C **79**, 481 (2019).

[62] G. Brooijmans *et al.*, Les Houches 2017: Physics at TeV Colliders New Physics Working Group Report, in *Les Houches 2017: Physics at TeV Colliders New Physics Working Group Report*, 2018, http://lss.fnal.gov/archive/2017/conf/fermilab-conf-17-664-ppd.pdf.